DISCRETE FREQUENCY SOUND RADIATION DUE TO FLUID FLOW OVER FLAT PLATES WITH ACOUSTICALLY NON-COMPACT CHORD

Makoto AOKI
Kawasaki Heavy Industries, Ltd., Technical Institute
1-1, Kawasaki, Akashi, Hyogo, 673-8666 Japan

Kunihiko ISHIHARA
The University of Tokushima, Department of Mechanical Engineering
2-1, Minamijosanjima-cho, Tokushima, 770-8506 Japan

Tomonobu GOTO
Tottori University, Department of Mechanical Engineering
Koyama, Tottori, 680-8552 Japan

Keywords: *aerodynamic sound, velocity dependency, directivity, plate, edge shape*

Abstract

The intensity and the directivity of discrete frequency sound generated from flat plates with various chord-to-thickness ratios and two types of edge shapes were investigated by wind tunnel experiments and numerical analyses. The experimental data indicated that as either a chord length becomes longer or wind velocity becomes larger, the intensity of aerodynamic sound is not simply proportional to the flow velocity to the sixth power (sixth power law) and the dipole type directivity pattern is biased toward upper stream direction. That is, the flat plate becomes acoustically non-compact even when the wind velocity is at very low Mach number. Numerical analyses for some plates were performed in order to be compared with the experimental data. A combined method was applied. That consists of a two-dimensional computational fluid dynamics (CFD) code based on the incompressible Navier-Stokes equations and a two-dimensional aero-acoustics code based on Lighthill's equation employing a Green's function tailored to the geometry of each flat plate. The calculated sound fields qualitatively agree with the experimental ones. Moreover, identification of sound source location was carried out by the numerical method. It was found that the effective Lighthill's sound source exists near the trailing edge, whatever the edge shape is. On the basis of these results, a simplified model to present the sound field around a non-compact plate is introduced. Furthermore, a practical criterion for compactness of a flat plate is proposed that the ratio of the chord to the acoustic wavelength is less than about 0.3.

1 Introduction

Aerodynamic sound occurs when a plate or an airfoil is put in a flow and often causes undesirable problems in fluid machinery system. The aerodynamic sound induced by periodic vortex shedding from the plate is referred to as discrete frequency sound since its frequency characteristic has a dominant peak of narrow-band. It has been known for many years that the vortex shedding frequency depends on the shape and the size of the plate as well as the wind velocity.

Discrete frequency sound aerodynamically generated from a flat plate has been studied in some papers [1,2,3]. The accumulation of aerodynamic sound data is crucial not only for investigation of sound characteristics but also for identification of aerodynamic force, which occasionally causes undesirable aero-elastic vibrations. However, it seems that the

systematic investigation based on wind tunnel experiments for various flat plates hardly has existed.

In this study, for the purpose of investigating the effect of chord-to-thickness ratio and edge shape of a flat plate on the discrete frequency sound, wind tunnel tests were performed for many sets of flat plates with c/t, where c and t are the chord length and the thickness of the flat plate, respectively. In some cases, the intensity of the discrete frequency sound did not increase with the wind velocity U according to the well-known U^6 law. Namely, for flat plates with longer chord length, the discrete frequency sound intensity increased in the complicated manner in which the index considerably deviates from six. This is because the scattering of sound by the plate itself makes the sound field around the plate complex if the chord length c is not much smaller than the characteristic sound wavelength λ (*i.e.*, the flat plate becomes acoustically non-compact).

For the evaluation of the aerodynamic sound generated from a rigid body, Curle's equation [4] is often applied because of its convenience. That is, in low Mach number flow, the aerodynamic force exerted on the body can be approximately evaluated by using far-field sound pressure and the dipole term of Curle's equation under the condition that the body can be regarded as acoustically compact [4]. If the body is not compact, the evaluation of the aerodynamic force using the sound pressure according to Curle's equation may lead to incorrect value. Hence, it is very important to examine a practical limit of c/λ under which a flat plate may be considered as acoustically compact.

In this paper, first, following four parameters concerning the discrete frequency sound generated from various flat plates are investigated through the wind tunnel tests: (i) Strouhal number St, (ii) wind velocity dependency, and (iii) directivity. In addition, (iv) practical c/λ limit of compact body approximation is evaluated according to our large number of experimental data on (ii). Next, the discrete frequency sound is also numerically obtained according to Lighthill's equation [5].

The calculated results qualitatively agree with the experimental ones. Then, the mechanism of aerodynamic sound generation is numerically investigated in detail since the validity of the present method has been confirmed. It is clarified that regardless of the edge shape the main contributor of Lighthill's sound source to the acoustic far field exists in the region close to the trailing edge. In addition, the sound field around a flat plate is reproduced by a simplified model consisting of a dipole source and the flat plate. The result reveals the effect of c/λ on the directivity pattern.

On the basis of these experimental and numerical results, we propose a practical and reasonable criterion of c/λ to judge the compactness of a flat plate. This threshold value is reasonably consistent with Howe's analytical result [6] for an airfoil with a finite chord length.

2 Wind Tunnel Experiments

2.1 Experimental Apparatus and Method

Experiments were carried out for flat plates with c/t ranging from 2.0 to 37.5 as summarized in Table 1. The total number of combinations of c/t was twenty-four. All the flat plates were made of steel and had a span-wise length of 200mm, which was adjusted to the height of the cross section of the open mouth of the wind tunnel. Two types of edge shapes, semi-circular and square, were adopted as either leading edge or trailing edge of flat plate. In this paper, the semi-circular edge shape is abbreviated to "R", and the square edge shape is abbreviated to "Sq". There are four combinations of the leading and trailing edges: (i)Sq-Sq, (ii)Sq-R, (iii)R-Sq, and (iv)R-R, where the manner of abbreviating plate geometry is as "leading edge - trailing edge".

Each of the plates was set in our low noise wind tunnel [7] of which test section was in anechoic chamber as illustrated in Fig. 1. The cross section of the nozzle was 200mm square. The wind velocity U at the test section was variable from 20 to 50m/s in 2m/s increments. The angle of attack was set zero degrees for

every test plate. At the longitudinal sides of the plate in span-wise direction, acoustically permeable end plates were set in order to reduce not only sound due to shear layers developed from the nozzle outlet, but also acoustic resonance due to sound reflection from the end plates [8]. By these end plates, two-dimensional flow field and low background noise field were reasonably secured. The turbulent intensity and the uniformity of the mean flow at the nozzle outlet were within 1.0%, respectively.

The amplitudes and phases of the aerodynamic sound pressure were recorded with a 1/2-inch microphone set up at a mid-span position of 0.5m away from a center of test plate with θ=0 degrees, where θ is the azimuth angle and zero degrees indicates the direction perpendicular to the mean flow, *i.e.*, the direction of lift force. As for some plates, the directivity of U=30m/s was also investigated at nine mid-span positions for r=0.5m with θ ranging from –30 to 50 degrees in 10 degrees increments. The measured sound pressure was analyzed by using FFT procedures, where its frequency resolution had 12.5Hz and its frequency range was up to 5000 Hz.

Table 1. Thickness and chord of test plates.(unit: mm)

| $t\backslash c$	20	30	40	50	60	75	100	110	120	130	140	150
4												
6												
8												
10												
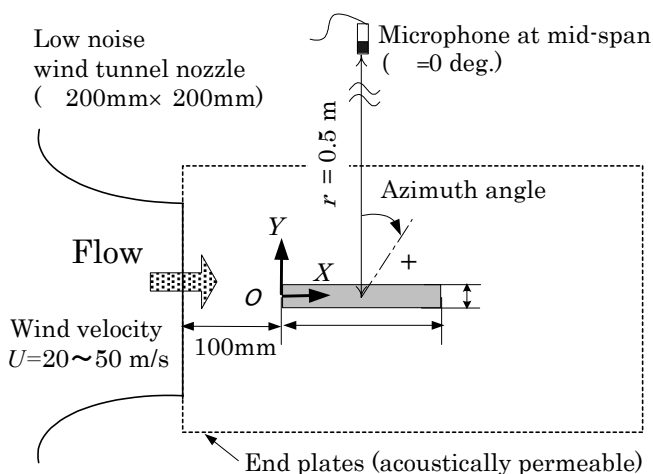
Fig.1 Schematic diagram of experimental apparatus.

2.2 Experimental Results and Discussions

2.2.1 Strouhal Number

The frequency characteristics of generated sound from the plates, "R-R" and "Sq-Sq", are shown in Fig. 2. For every plate, apparent discrete frequency sound was observed. Hereafter, only a dominant peak component in each spectrum is dealt with. Some of the wind velocity dependencies of the peak frequency f_p are shown in Fig. 3. The general trend observed in Fig. 3 is that f_p is lineally and continuously increased with U. The proportional constants of the approximate lines in Fig. 3 can yield the identification of average Strouhal number St, which is defined as $St = f_p\, t\, /\, U$, for U=20 to 50m/s.

The variations in St with c/t shown in Fig. 4 are divided into two groups, such as (i) Sq-Sq,
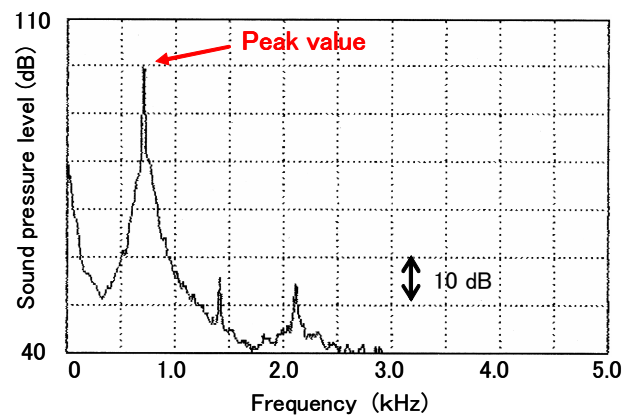
(a) Case of R-R plate
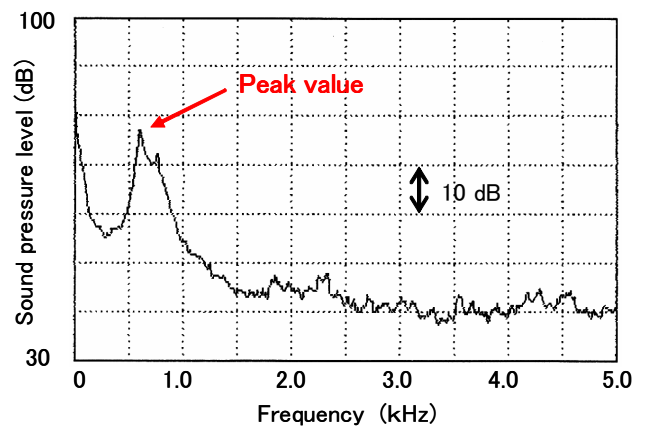
(b) Case of Sq-Sq plate

Fig.2 Spectra of measured sound pressure. (t=10mm, c=150mm, U=30m/s, θ=0deg.)

Sq-R and (ii) R-R, R-Sq. The former has square leading edge and indicates St 0.2 for c/t 25, the latter has semi-circular leading edge and indicates St 0.2 for c/t 25. Namely, St depends on the leading edge shape in this range of c/t. In contrast, on condition that c/t >25, asymptotic value of St for both (i) and (ii) becomes about 0.2. Above trend almost corresponds to the data shown in Ref. [2].

2.2.2 Dependency of Peak SPL on Wind Velocity

The dependencies of peak sound pressure level (*Peak SPL*) on wind velocity are shown in Figs. 5(a) - 5(d) for several c/t, where the solid lines in Fig. 5 are the polynomial approximations identified by the least-squares method.
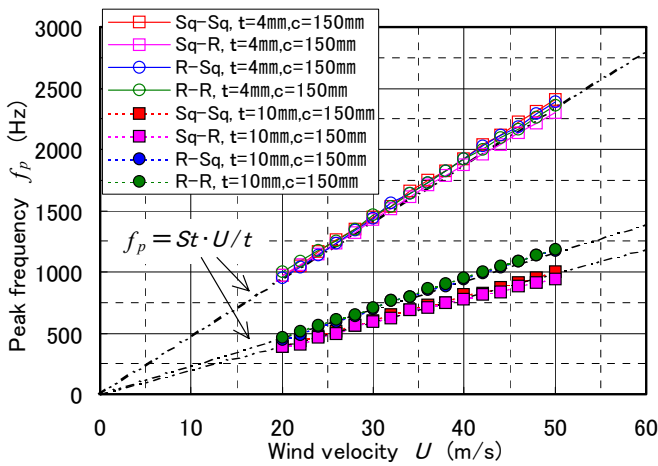

Fig.3 Peak frequency f_p vs. wind velocity U.
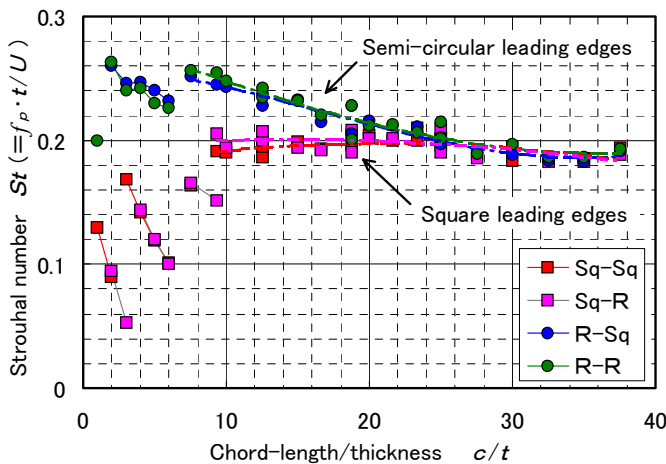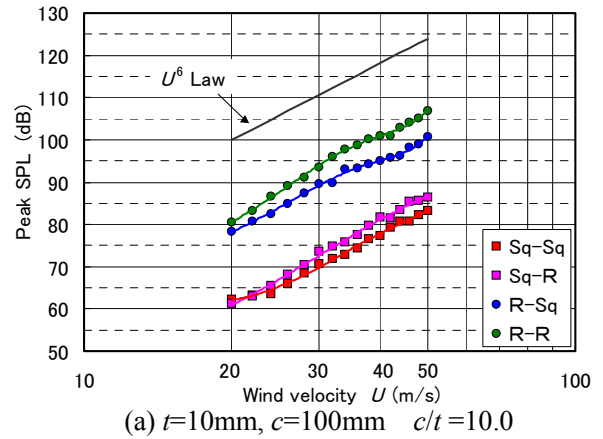(t=4mm, c=150mm and t=10mm, c=150mm.)
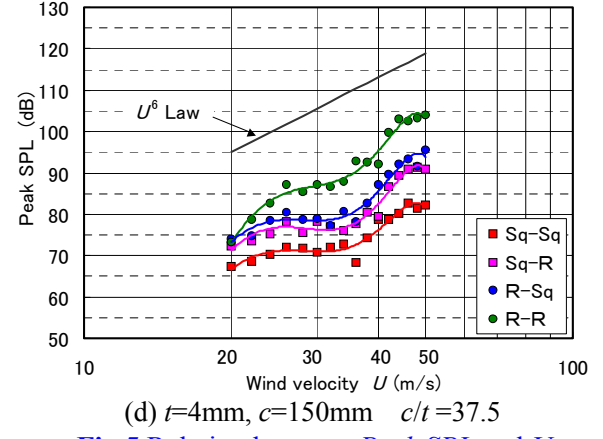

Fig.4 Relation between St and c/t for various edges.

(a) t=10mm, c=100mm c/t =10.0
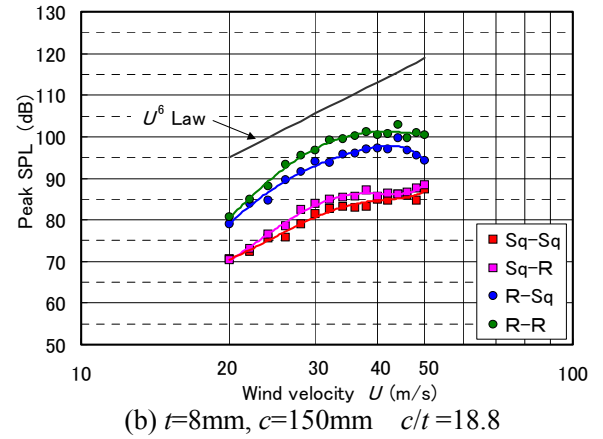
(b) t=8mm, c=150mm c/t =18.8
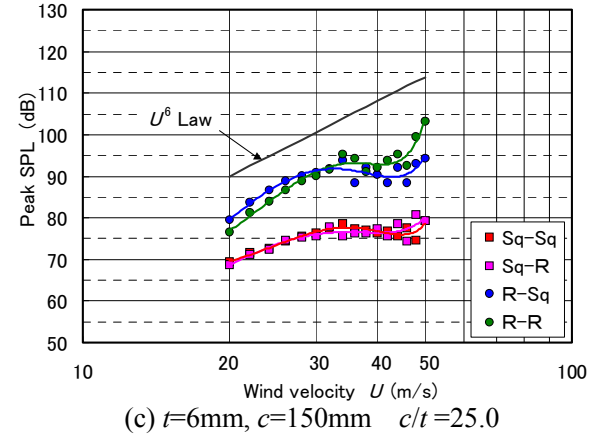
(c) t=6mm, c=150mm c/t =25.0

(d) t=4mm, c=150mm c/t =37.5

Fig.5 Relation between *Peak SPL* and U.
(Experiment, r=0.5m, θ=0 deg.)

Peak SPL in Fig. 5(a) increases according to the U^6 law such as aeolian tone from a circular cylinder [9], while Figs. 5(b) - 5(d) with c/t sparsely ranging from 18.8 to 37.5 show that the increase in *Peak SPL* with U obeys not the U^6 law but rather oscillatory polynomial curve. In addition, it can be seen that in the case of the same c/t for Fig. 5 the increase in *Peak SPL* shows remarkably similar tendency although each plate has different edge shape. Moreover, it has been confirmed by authors that the wind velocity dependency at r=1.0m, which has been investigated separately and not shown here, is the same as that at r=0.5m in Fig. 5. Thus, there is only slight difference in the velocity dependency whether in near field or in far field away from the plate.

At first, the resonance relating to the experimental apparatus had been suspected of causing the complicated velocity dependency shown in Figs. 5(b) - 5(d). There had been two types of possible resonators, the interval of the acoustically permeable end plates and the nozzle outlet space of the wind tunnel. Acoustic experiments of speaker excitation carried out for the relevant parts demonstrated that no interfering resonance existed in the apparatus.

The dependence of the flow field around the plate on the velocity had been supposed as another cause of the complicated *Peak SPL* increment. (That is, it was expected that the similarity of the flow field with U had been not ensured in the experiments.) However, since the wind velocity U at which *Peak SPL* begins to deviate from the U^6 law is similar for plates with the same c/t regardless of edge shape (*i.e.,* flow field) as shown in Figs. 5(b) - 5(d), we deduced that the complicated velocity dependency of the discrete frequency sound is mainly due to an acoustical phenomenon. Namely, that complexity appears when the flat plate becomes acoustically non-compact (*i.e.*, c is not much smaller than λ) as c/t becomes large.

On the basis of our experimental results for all plates summarized in Table 1, under the condition c/t 15, *Peak SPL*'s increment begins to deviate from the U^6 law. The threshold value of the ratio at which a flat plate can be

considered as to be acoustically compact is c/t=15 in the range U 35m/s.

The relation between c/λ and c/t is given by Eq. (1).

$$c / \lambda \quad St \quad U / a_0 \quad c / t \qquad (1)$$

Hence we obtain c/λ=0.31 $1/\pi$ as the threshold value for compactness of a flat plate, substituting U=35m/s, a_0=340m/s, c/t=15, and St=0.2, which is the average value of our experiments. Here, a_0 is the speed of sound in fluid at rest. This threshold is in good agreement with that obtained by numerical analysis as referred in Sec.4.2.

(a) Case of R-R plate

(b) Case of Sq-Sq plate
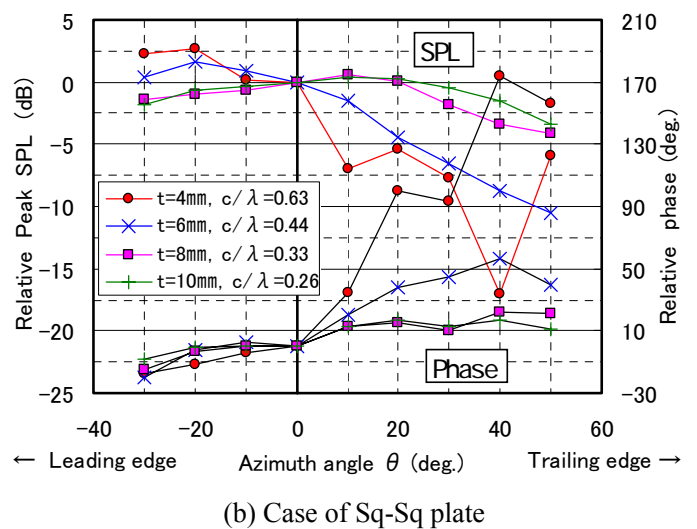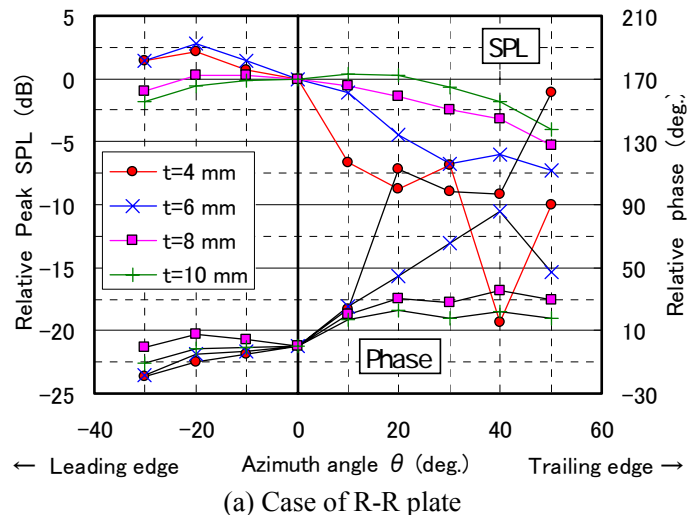
Fig.6 Directivity of aerodynamic sound generated from plates. (Experiment, c=150mm, U=30m/s.)

2.2.3 Directivity of Peak SPL

The directivity patterns of *Peak SPL* for *c*=150mm are shown in Fig. 6. Both *Peak SPL* and its phase values in Fig. 6 are described as relative values with reference to those at *θ*=0 degrees (see Fig. 1). We have confirmed that the distributions of *Peak SPL* are symmetrical and those of phase are 180 degrees out-of-phase with *Y*=0 (although the data are not shown here).

The relative *Peak SPL* in Figs. 6(a) and 6(b) shows that the directivity pattern such as dipole type is biased toward upper stream direction, *i.e.*, leading edge side (*θ*<0 deg.), as *t* becomes small. As for the variation in *Peak SPL* with *θ*, trailing edge side is more sensitive than leading edge side. In addition, the relative phase in Figs. 6(a) and 6(b) shows that its variation with *θ* becomes large as *t* becomes small. Moreover, the point that should be paid attention is to be found little difference in comparison of directivity characteristics between Fig. 6(a) of "R-R" and Fig. 6(b) of "Sq-Sq". Thus, it is expected that the radiation directivity scarcely depends on either the leading or trailing edge shape.

According to these experimental results, the wind velocity dependencies of the sound resemble each other if the plates have the same *c*/*t* regardless of the edge shape, and so do the directivity patterns. This suggests that the *c*/*t* (*i.e.*, *c*/*λ*, compactness) dominates the two characteristics, and that, from an acoustical point of view, the effective sound source for a flat plate is distributed in a similar region independently of the edge shape.

3 Numerical Analyses

3.1 Aerodynamic Sound Analysis Method

A combined method which consists of a two-dimensional computational fluid dynamics (CFD) code and a two-dimensional aero-acoustics code is applied to numerical analyses. In our experiments, the flow field around the flat plate was nearly two dimensional and the Mach number of the flow was very low, *i.e.*, $M=U/a_0$ 0.15. In order to solve the two dimensional incompressible Navier-Stokes

(a) Global domain
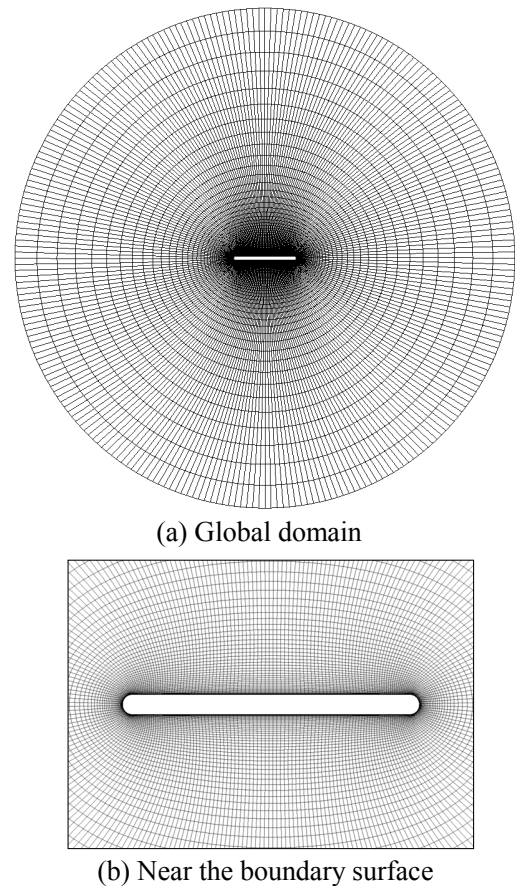

(b) Near the boundary surface

Fig.7 Grid system for two-dimensional CFD analysis.

equations, we employ a CFD code, "Nag2dgh" [10], which adopts a numerical scheme suitable for unsteady flow calculation without any turbulence models.

The grid system for CFD analysis has O-type topology as shown in Fig. 7 and the whole grid contains 256 points in the circumferential direction, 64 points in the radial direction, representing a total of 16384 points. A non-dimensional distance from the boundary surface to the nearest grid point is about $0.1/Re^{0.5}$, where *Re* is the Reynolds number and defined as *Re* = *U t* /*v*, and *v* is the kinematic fluid viscosity. For the purpose of qualitative estimations for flow field around the flat plate, the calculation Reynolds number for all plates is retained in the same value, *Re*=20000, assuming that *U*=30m/s and *t*=10mm.

As for aero-acoustic analysis, the Lighthill's equation [5] combining a Green's function tailored to a rigid body geometry is used [11],

because we have to estimate the sound field from acoustically non-compact plate in spite of using the incompressible flow calculation results [12,13]. In the case of our study, since it seems that both the flow and sound field due to the periodic vortex shedding are quasi time harmonic, the analytical solution of sound pressure p' is obtained using the Lighthill's equation with time harmonic expression and is given by

$$p'(\mathbf{x}, \boldsymbol{\omega}) = \int_{V(\mathbf{y})} G^{\boldsymbol{\omega}} \frac{\partial^2 T_{ij}^{\boldsymbol{\omega}}}{\partial y_i \partial y_j} dV(\mathbf{y}) \quad \frac{\partial G^{\boldsymbol{\omega}}}{\partial n} = 0 \; on \; S(\mathbf{y}), \quad (2)$$

where: $\mathbf{x}$ is the observer position, $\mathbf{y}$ is the source position within the flow field, ω is the angular frequency ($=2\pi f$), G is the acoustic Green's function tailored to the plate geometry, T_{ij} is the Lighthill's stress tensor, the superscript ω denotes the Fourier transform with respect to time, $S(\mathbf{y})$ is the surface of the plate, and n is the unit normal vector on S. For flows at low Mach number and high Reynolds number such as our study, the T_{ij} approximately reduces to $\rho_0 v_i v_j$ [5], where ρ_0 is the medium density in fluid at rest.

For the purpose of qualitative and reasonable estimations for sound field, we apply the two-dimensional boundary element method (BEM) for Helmholtz equation to the calculation of G^{ω} in Eq. (2). In this study, BEM is based on constant elements scheme in order to avoid a corner singularity problem [14] and employs the CFD grid as it is. The integral in Eq. (2) is taken over the volume $V(\mathbf{y})$ involving whole flow calculation result.

The fundamental solution G_0^{ω} (*i.e.*, free space Green's function) for two-dimensional Helmholtz equation is [14]

$$G_0^{\boldsymbol{\omega}}(\mathbf{x}, \mathbf{y}) = -\frac{j}{4} H_0^{(2)}(kr), \quad (3)$$

where j is the imaginary unit ($j^2 = 1$), $H_0^{(2)}$ is the second kind Hankel function of zeroth order, $k=\omega/a_0$ is the acoustic wave number, and $r = |\mathbf{x} \quad \mathbf{y}|$. It is well known for the Helmholtz equation that the reciprocal theorem is satisfied and the following relation holds: $G^{\omega}(\mathbf{x},\mathbf{y}) = G^{\omega}(\mathbf{y},\mathbf{x})$. Therefore, we substitute the G^{ω} obtained by setting a point source at $\mathbf{x}$ into that in Eq. (2) because of the remarkable

improvement of calculation speed [11]. Note that Eq. (2) can be used to evaluate the near-filed sound pressure as well as the far-filed pressure if $p' = a_0^2(\rho \quad \rho_0)$, since the assumption such as neither $|\mathbf{x}| \quad \lambda$ nor $|\mathbf{x}| \quad c$ is included in the present method.

When $|\mathbf{x}|$, G_0^{ω} is expressed as:

$$G_0^{\boldsymbol{\omega}}(\mathbf{x}, \mathbf{y}) \approx \frac{1}{j} \sqrt{\frac{1}{8\boldsymbol{\pi} kr}} \exp[-j(kr - \frac{\boldsymbol{\pi}}{4})] . \quad (4)$$

From Eq. (4), we find $|G_0^{\omega}| \quad (\omega r)^{-0.5}$ and its relation is different from $|G_0^{\omega}| \quad r^{-1}$ for three-dimensional field. Thus, as for following calculated *Peak SPL* with the velocity dependency in Sec.3.3.2 and Sec.4.2, a correction, " $10 \log_{10} \omega$", is applied so that $|G_0^{\omega}|$ is not influenced by the change in ω like the three-dimensional field.
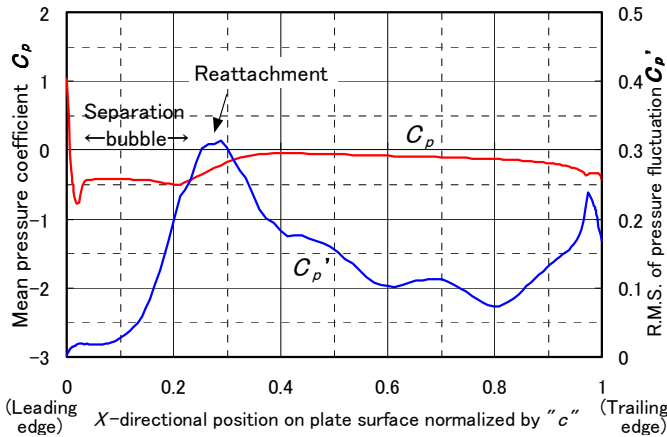
3.2 Results of Flow Field Calculation

Figure 8 shows the iso-contours of calculated instantaneous vorticity around two flat plates "R-R" and "Sq-Sq" with t=10mm and c=150mm. These results indicate that the shear layer separated from the leading edge reattaches at the mid-chord position or upper-stream point, and that the periodic vortex shedding from the trailing edge is generated.
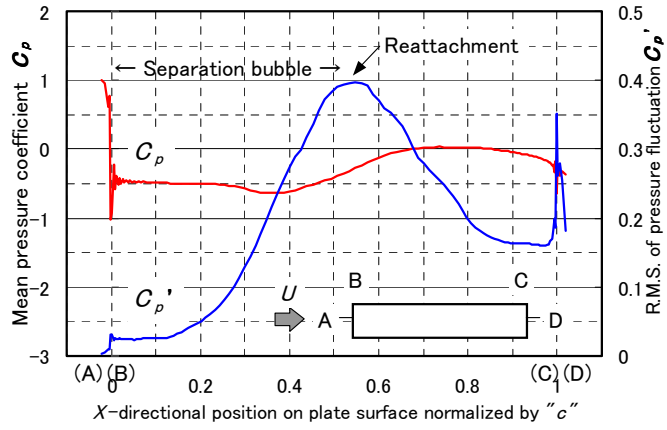
Figure 9 shows the surface pressure distributions on one side of the same plates shown in Fig. 8. It was found that R.M.S. of the

Flow

(a) Case of R-R plate

.... : Clockwise
———— : Counter clockwise
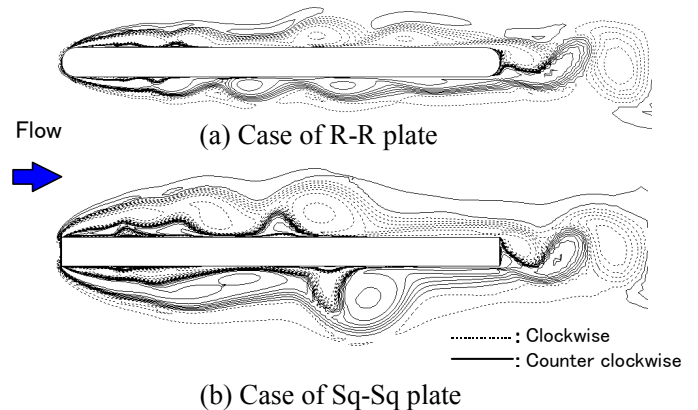
(b) Case of Sq-Sq plate

Fig.8 Instantaneous iso-vorticity contours.
(Analysis, t=10mm, c=150mm, Re=20000.)

(a) Case of R-R plate
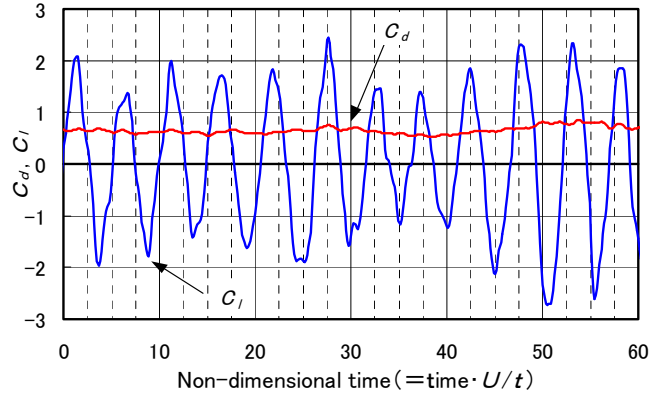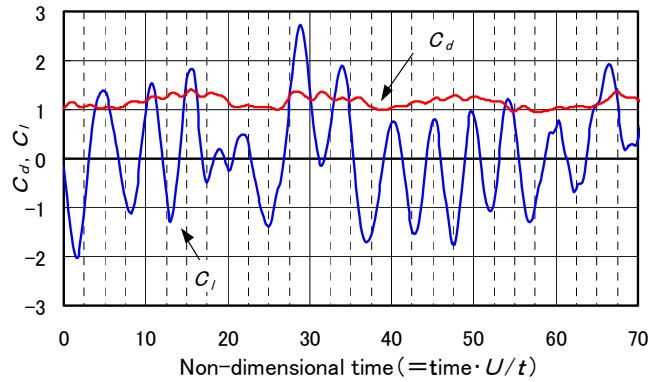

(b) Case of Sq-Sq plate

Fig.9 C_p and C_p' on the plate surface of one side.
(Analysis, t=10mm, c=150mm, Re=20000.)

(a) Case of R-R plate

(b) Case of Sq-Sq plate

Fig.10 Time history of C_d and C_l.
(Analysis, t=10mm, c=150mm, Re=20000.)

3.3 Results of Sound Field Calculation

3.3.1 Spectrum of SPL

Figure 11 shows the calculated spectra of SPL with t=10mm, c=150mm, and U=30m/s for "R-R" and "Sq-Sq". It is assumed that simultaneous vortex shedding occurs along the span-wise direction of the plate of L=200mm and the flow field is uniform in this direction. In order to make a comparison, the calculation result based on Curle's equation (5), which has the dipole term only and is obtained by using Eq. (3) as G_0^ω for two-dimensional form, is also plotted in Fig. 11.

$$p'(\mathbf{x}, \omega) = \frac{jk}{4} \int_{S(\mathbf{y})} \frac{x_i - y_i}{r} H_1^{(2)}(kr) n_i P(\mathbf{y}, \omega) dS(\mathbf{y}), \quad (5)$$

where P is the surface pressure on the plate, and $H_1^{(2)}$ is the second kind Hankel function of first order.

pressure coefficient fluctuations C_p' becomes large at the reattach position of separation bubble. The trend for both C_p and C_p' in Fig. 9 is qualitatively in agreement with experimental data [15].

Figure 10 shows the time histories of the drag coefficient C_d and the lift coefficient C_l with the same plates as Figs. 8 and 9, where these force coefficients are normalized by the dynamic pressure of mean flow and the plate thickness, i.e., $0.5\rho_0 U^2 t$. Fig. 10 reveals that the variation in C_l is almost periodic as considered in Sec.3.1 and suggests the presence of regular vortex shedding like the Karman vortex street from a cylinder.

Table 2. *St* for R-R Plates. (Analysis vs. experiment)

Plate spec. (*c*=150mm)	*t* =4	*t* =6	*t* =8	*t* =10
Analysis	0.16	0.17	0.18	0.20
Experiment	0.19	0.22	0.23	0.23

Table 3. *St* for Sq-Sq Plates. (Analysis vs. experiment)

Plate spec. (*c*=150mm)	*t* =4	*t* =6	*t* =8	*t* =10
Analysis	0.15	0.15	0.18	0.18
Experiment	0.19	0.20	0.20	0.20

(a) Case of R-R plate

(b) Case of Sq-Sq plate
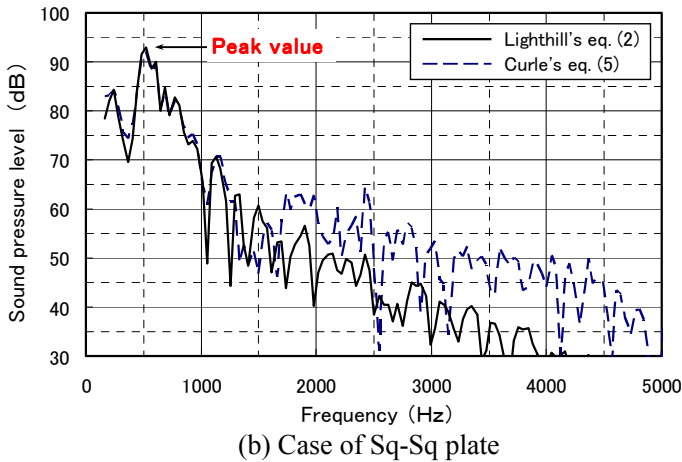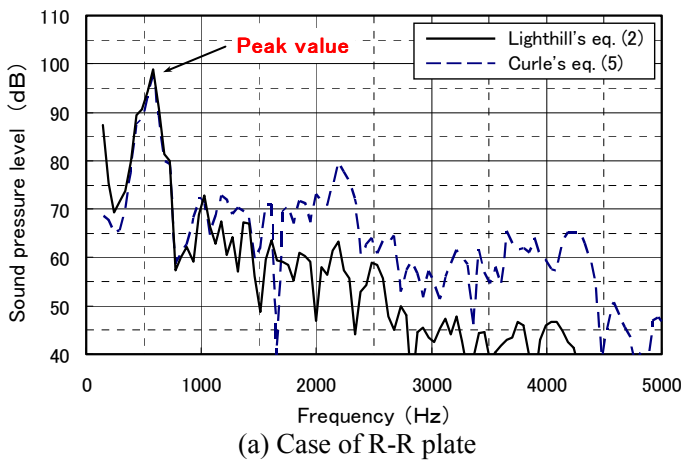
Fig.11 Spectra of calculated SPL.
(*t*=10mm, *c*=150mm, *U*=30m/s, *r*=0.5m, *θ*=0deg.)

Fig.12 Relation between *Peak SPL* and *U*.
(Analysis, Sq-Sq, *c*=150mm, *θ*=0deg.)

Each of the calculated SPL spectra in Fig. 11 has one dominant frequency peak similar to the experimental spectra shown in Fig. 2. The analyzed *St* numbers summarized in Tables 2 and 3, which are obtained from each f_p, are about 15 to 20% smaller than experimental

values because of the coarseness of the CFD grid, however, the tendency such that *St* becomes smaller as the plate thickness becomes thinner is similar to the experimental one. A comparison of the Lighthill's solution with Curle's result shown in Fig. 11 indicates that while *Peak SPL* values match fairly well, there is greater discrepancy in SPL as the frequency is higher. This is because the flat plate becomes acoustically non-compact in the higher frequency region and the Curle's solution using the incompressible surface pressure may lead to correct value no longer.

3.3.2 Wind Velocity Dependency

Figure 12 shows examples of the velocity dependencies of calculated *Peak SPL* for "Sq-Sq" plates. Here, the T_{ij} is calculated from the data of the flow velocity field of *Re*=20000 for all *U*. As shown in Fig. 12, the increase in *Peak SPL* with *U* obeys not the U^6 law but rather oscillatory polynomial curve as *t* becomes small. This trend qualitatively corresponds to the experimental one shown in Figs. 5(b) - 5(d). Moreover, from a comparison between at *r*=0.5m and at *r*=5.0m in Fig. 12, it can be said that the velocity dependency hardly depends on the distance *r*. However, the velocity at which *Peak SPL* begins to deviate from the U^6 law in Fig. 12 is higher than the experimental one, because the analyzed *St* is smaller than

experimental one. In addition, according to the "R-R" calculation result, which is not shown here, the velocity dependency of "R-R" fairly resembles that of "Sq-Sq" likewise the experimental trend does.

Since the calculated velocity dependency, which is based on the assumption that the velocity field is the same for any U, qualitatively corresponds to the experimental result such that *Peak SPL* deviates from the U^6 law as t becomes small, we conclude that c/λ dominates the velocity dependency.

3.3.3 Directivity

Figure 13 shows examples of the calculated directivity patterns of *Peak SPL* for "Sq-Sq" plates, where the wind velocity in this figure is defined as $U=30/0.8 \approx 37.5$m/s in order to adjust f_p to the same value with experiment since the analyzed St numbers are about 20% smaller than the experimental ones. The calculated directivity in Fig. 13 is in good agreement with the experimental one shown in Fig. 6(b). Moreover, from a comparison between at $r=0.5$m and at $r=5.0$m in Fig. 13, it can be said that the directivity hardly depends on the distance r. Concerning the directivity of the "R-R" plate and "Sq-Sq" plate, the similarity observed in the experimental results is confirmed though the "R-R" result which is not shown here.

3.3.4 Discussions

The calculation results of the two characteristics of the sound, the velocity dependency and the directivity, qualitatively correspond to the experimental ones even though the calculated flow velocity field is the same for any U. Also, the two characteristics are fairly similar for plates with the same c/t regardless of plate geometries as is found in the experiments. From an acoustical point of view, the effective sound source for a flat plate is supposed to be distributed in a similar region independently of the edge shape.

These facts indicate that c/λ essentially dominates both characteristics. When c/λ becomes large (*i.e.*, the flat plate becomes acoustically non-compact), the sound scattered

by the plate results in the complicated sound field and causes the velocity dependency to be complicated.

4 Sound Source and Scattered Sound Field

4.1 Distributions of Lighthill's Sound Source

In this section, we investigate the Lighthill's sound source $\partial^2 T_{ij}^{\omega}/\partial y_i \partial y_j$ distributions in the calculated flow field. This is a complex number and is abbreviated to $T_{ij}^{\omega}{}''$ hereafter.

Figure 14 shows the distributions of $|T_{ij}^{\omega}{}''|$ at f_p for $t=10$mm and $c=150$mm, and $|T_{ij}^{\omega}{}''|$ is symmetrically distributed with respect to $Y=0$. As for comparison of phase distributions of $T_{ij}^{\omega}{}''$ between upper and lower side of the plate, its difference is about 180 degrees (not shown here), which fundamentally makes the directivity pattern a dipole type.

As shown in Fig. 14, the large values of $|T_{ij}^{\omega}{}''|$ exist in both the reattached region of separation bubble (see label 'A' in Fig. 14) and the shed region of periodic vortex (see label 'B' in Fig. 14). Since 'A' and 'B' in Fig. 14 are close to the areas on the plate surface where C_p' show local maxima in Fig. 9, there may be a strong correlation between $|T_{ij}^{\omega}{}''|$ and C_p' in this study.
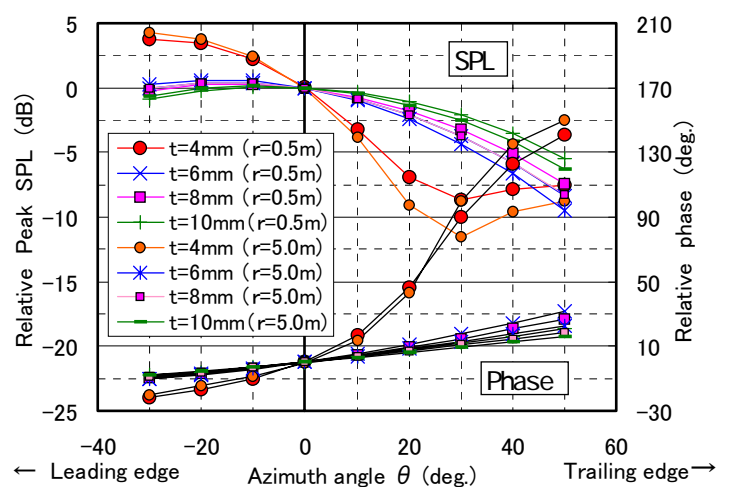

Fig.13 Directivity of aerodynamic sound generated from plates. (Analysis, Sq-Sq, $c=150$mm, $U=37.5$m/s.)

Table 4. Investigation results of source contribution for "R-R".

Plate spec. c=150	SPL SPL	$20 \, Log_{10} \, \sigma$ at f_p		$20 \, Log_{10}$ $(|A|/|B|)$*
		Region A	Region B	
t=4	23 dB	36 dB	28 dB	25 dB
t=6	18 dB	48 dB	26 dB	0 dB
t=8	12 dB	47 dB	24 dB	3 dB
t=10	9 dB	46 dB	22 dB	5 dB

* |A| and |B| mean $\int |T_{ij}^{\omega}{}''| \, dV$ for Region A and B, respectively.

(a) Case of R-R plate

(b) Case of Sq-Sq plate
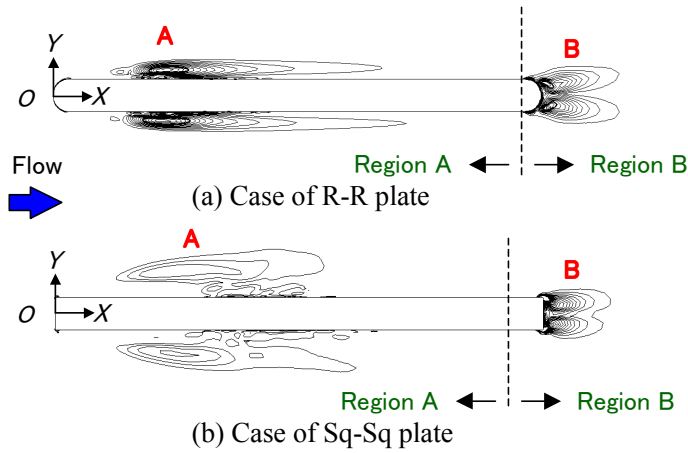
Fig.14 Lighthill's sound source $|T_{ij}^{\omega}{}''|$ distributions at f_p. (Analysis, t=10mm, c=150mm, Re=20000.)

The investigation results of contribution of $T_{ij}^{\omega}{}''$ to far-field *Peak SPL* are summarized in Table 4 for "R-R" plates. Here, SPL_A and SPL_B in Table 4 indicate *Peak SPL* by volume integration in Eq. (2) with respect to 'Region A' and 'Region B' in Fig. 14, respectively. The condition of SPL evaluation is U=30m/s, r=0.5m, and θ=0 degrees. The effective strength of sound source $T_{ij}^{\omega}{}''$ for each region, σ in Table 4, is defined by Eq. (6):

$$\sigma = \frac{\left| \int T_{ij}^{\omega}{}'' dV \right|}{\int \left| T_{ij}^{\omega}{}'' \right| dV} \quad for \quad Y \geq 0 \; . \quad (6)$$

Since "$SPL_A \; SPL_B$" in Table 4 are negative for all plates, the contribution of 'Region A' is smaller than that of 'Region B'. Also, "$20Log_{10}\sigma$" in Table 4 indicates that 'Region A' is much smaller than 'Region B' for all plates. Namely, $T_{ij}^{\omega}{}''$ in 'Region A' hardly contributes to the acoustic far field owing to a cancellation mechanism based on steep variation in the phase of 'Region A', the reattached region. As a result, it was found that the effective sound source exists in the neighborhood of the trailing edge
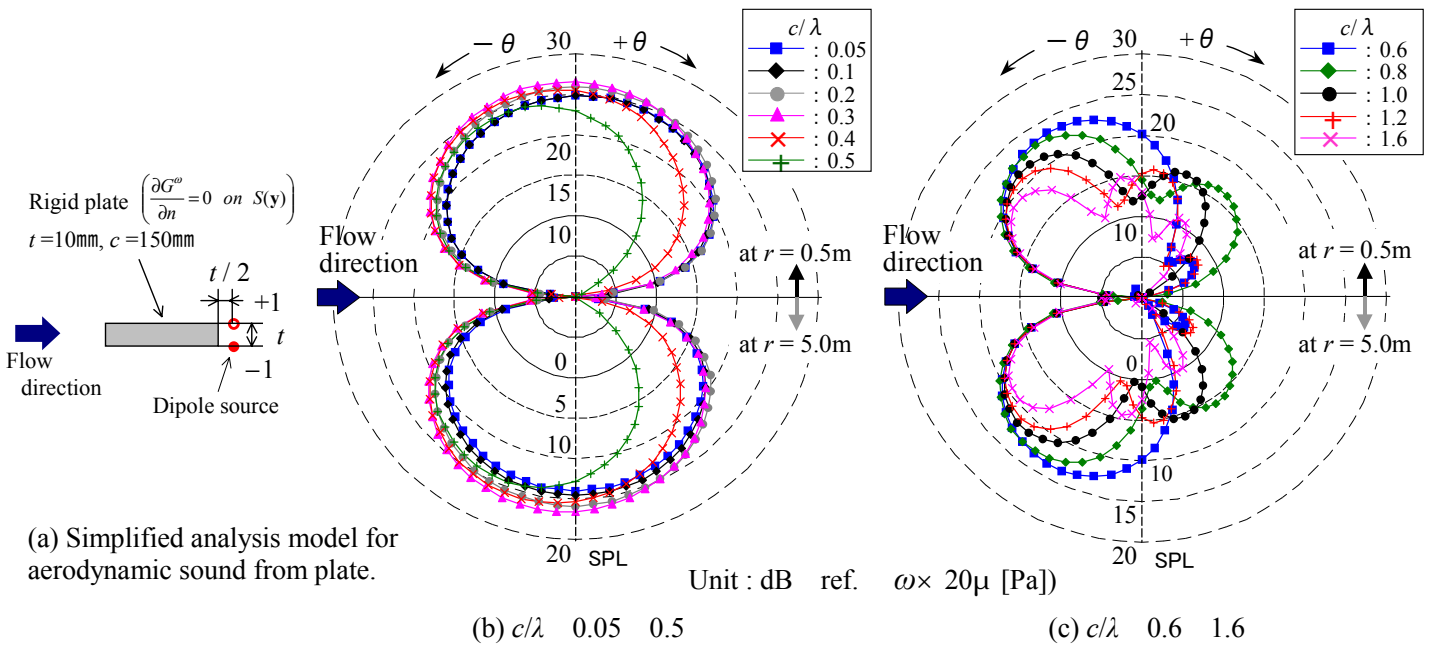
as examined for broad band sound [16]. We have confirmed the same for the "Sq-Sq" plates (the data are not shown here). The effective sound source exists near the trailing edge independently of the plate geometry.

4.2 Scattered Sound Field Analysis by Simplified Aerodynamic Sound Model

From the above discussions, we found that the effective sound source of aerodynamic sound from a plate exists near the trailing edge. Thus, in this section, we investigate the effect of c/λ on the sound field around a flat plate by use of a simplified two-dimensional BEM acoustic model consists of a dipole source near the trailing edge and the plate as illustrated in Fig. 15(a).

The dipole source in Fig. 15(a), which consists of two mono-poles with unit strength and out-of-phase each other, is located in typical position as adjusted to $|T_{ij}^{\omega}{}''|$ distributions for "R-R" and "Sq-Sq" shown in Fig. 14. The flat plate is assumed to be "Sq-Sq", t=10mm, and c=150mm. Here, the sound fields around the plate are calculated by substituting the plate surface pressure obtained from acoustic BEM analysis (*i.e.*, compressible pressure) into Curle's equation (5), because it is known that 'incident sound' from essential source (*i.e.*, dipole source in this model) is usually negligible compared to 'scattered sound' for low Mach numbers [12] and we just have to evaluate the 'scattered sound' field.

Figures 15(b) and 15(c) show the calculated directivity patterns of SPL with c/λ ranging from 0.05 to 1.6, where the upper side of the plate indicates the sound field at r=0.5m (near field) while the lower side indicates at r=5.0m (far field), because the SPL directivity in this study is exactly symmetrical with respect to Y=0. In addition, a dipole source makes the far-field sound pressure "$p' \; \omega$", and G_0^ω in two-dimensional field becomes $|G_0^\omega| \quad (\omega r)^{-0.5}$. Thus, we obtain "$p' \; \omega^{0.5}$". Hence, the correction, "$ 10Log_{10}\omega$", is made to SPL in Fig. 15 so as to get rid of the influence of ω on p'. This leads SPL directivity pattern to become

(a) Simplified analysis model for aerodynamic sound from plate.

(b) c/λ　0.05　0.5

(c) c/λ　0.6　1.6

Unit : dB　ref.　$\omega \times 20\mu$ [Pa])

Fig.15 Directivity of scattered sound pressure field consisting of dipole and rigid plate for various c/λ at r=0.5m and 5.0m. (Two-dimensional acoustic analysis by acoustic BEM and Curle's equation (5).)

similar regardless of ω when the directivity has a dipolar nature and the increase in *Peak SPL* with U obeys the U^6 law (*i.e.*, the flat plate is acoustically compact).

As for c/λ　0.3 in Fig. 15(b), the directivity patterns coincide with typical dipole form and the variation in SPL at θ=0degrees (*i.e.*, lift direction) with an increase in c/λ is 1 to 2 dB at most. On the other hand, as for c/λ　0.4 in Figs. 15(b) and 15(c), the direction of maximum SPL is more tilted toward the leading edge direction and the directivity pattern becomes more complicated with multiple lobes, as c/λ increases more. Thus, in the case of aerodynamic sound, since c/λ usually increases with an increase in U, an observer fixed in the lift direction repeatedly experiences the rise and fall of directivity lobes, which consequently causes the velocity dependency to become complicated as shown in Fig. 16, whether in near field or in far field from the plate. For example, the directivity for the plate with t=4mm and c=150mm shown in Fig. 6 and Fig. 13 is different from other three plates. This is because the directivity characteristic for c/λ=0.63 is about to change from dipolar into quadrupolar nature as shown in Fig. 15(c).
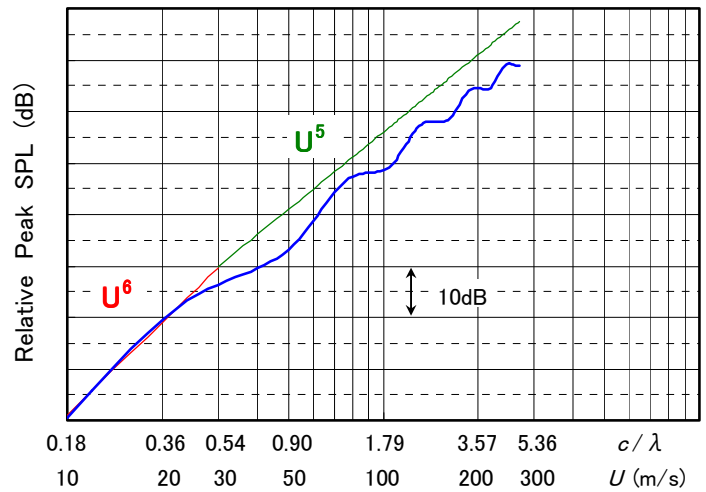
Fig.16 Wind velocity dependency up to high c/λ value. (Analysis by Lighthill's equation (2), R-R, t=4mm, c=150mm, r=0.5m, θ=0deg.)

From the above calculation results, the criterion such that the directivity characteristic does not satisfy the dipolar nature (*i.e.*, the flat plate becomes acoustically non-compact), is practically $c/\lambda > 0.3$. This threshold is in good agreement with that determined by the experiments as referred in Sec.2.2.2. In addition, even though the details are omitted here, we have confirmed that both the directivity pattern

and the threshold value don't change even if the location of the dipole source or the edge shape or c/t slightly changes from Fig. 15(a). Thus, we conclude that the threshold is c/λ=0.3. Besides, our proposed compactness criterion is also reasonably consistent with Howe's analytical result [6] for an airfoil with a finite chord length.

5 Conclusions

In this study, we examined the characteristics of the discrete frequency sound generated from flat plates with various c/t and edge shapes by the wind tunnel tests. The wind velocity dependency and the directivity were investigated not only by the experiment, but also by sound calculation based on Lighthill's equation. In addition, we considered the effective sound source location and the effect of c/λ on the sound field around a flat plate. As a result, the following conclusions are obtained:

(1) From a lot of experimental results of the velocity dependency and the BEM acoustic analysis based on the simplified aero-acoustic model, the proposed criterion for compactness of a flat plate (*i.e.*, the increase in *Peak SPL* with U obeys the U^6 law) is practically c/λ 0.3

   $1/\pi$, whether in near field or in far field. As c/λ becomes greater than this threshold value 0.3, the velocity dependency becomes more complicated, because the directivity pattern gradually changes from dipole into multi-pole.

(2) As for our experimental and calculation results, in the case of the same c/t plate, the trend of velocity dependency and directivity are similar independently of the edge shape. Thus, from an acoustical point of view, it was expected that the effective sound source for a plate is distributed in a similar region regardless of the edge shape. As a result of investigation of the Lighthill's sound source distributions around the plate, it was found that the effective sound source exists in the neighborhood of the trailing edge independently of the plate geometry as said so far.

References

[1] F.S.Archibald, "Self excitation of an acoustic resonance by vortex shedding," *Journal of Sound and Vibration*, 38(1), pp.81-103, 1975.

[2] R.Parker, and M.C.Welsh, "Effects of sound on flow separation from blunt flat plates,*" Int. Journal of Heat and Fluid Flow*, Vol.4-No.2, pp.113-127, 1983.

[3] W.K.Blake, "*Mechanics of flow-induced sound and vibration,Vol.2:Complex flow-structure interactions*," Academic Press., pp.718-836, 1986.

[4] N.Curle, "The influence of solid boundaries upon aerodynamic sound," *Proc. Roy. Soc.,* Ser.A 231, pp.505-514, 1955.

[5] M.J.Lighthill, "On sound generated aerodynamically I. General theory," *Proc. Roy. Soc.,* Ser.A 211, pp.564-587, 1952.

[6] M.S.Howe, "Edge-source acoustic Green's function for an airfoil of arbitrary chord, with application to trailing-edge noise," *Quarterly Journal of Mechanics and Applied Mathematics*, 54(1), pp.139-155, 2001.

[7] K.Ishihara, and M.Aoki, "Effect of splitter plate on generation mechanism of aeolian tones", 6th AIAA/CEAS Aeroacoustics Conference and Exhibit, Lahaina, Hawaii, AIAA Paper.2000-1983, 2000.

[8] H.Fujita, W.Sha, H.Furutani, and H.Suzuki, "Experimental investigations and prediction of aerodynamic sound generated from square cylinders," 4th AIAA/CEAS Aeroacoustics Conference, Toulouse, France, AIAA Paper.98-2369, 1998.

[9] O.M.Phillips, "The intensity of aeolian tones," *Journal of Fluid Mechanics*, 1, pp.607-624, 1956.

[10] H.Suito, K.Ishii, and K.Kuwahara, "Simulation of dynamic stall by multi-directional finite-difference method," 26th AIAA Fluid Dynamics Conference, San Diego, CA, AIAA Paper.95-2264, 1995.

[11] H.Kawazoe, Y.Nakamura, and Y.Ikeda, "Prediction of sound generation from flow field of axisymmetric jet with circular plate edge inserted in the shear flow," 3rd ASME/JSME Joint Fluids Engineering Conference, San Francisco, California, FEDSM 99-7235, 1999.

[12] M.S.Howe, "Trailing edge noise at low Mach numbers," *Journal of Sound and Vibration*, 225(2), pp.211-238, 1999.

[13] M.E.Goldstein, "*Aeroacoustics*," McGraw-Hill, 1976.

[14] C.A.Brebbia, "*The boundary element method for engineers*," Pentech Press., London, 1978.

[15] H.Muramatsu, Y.Tomita, and S.Inagaki, "A study of noise generated by separated flow (3rd report, The relationship between noise reduction of the flat plate and flow field)," Journal of Turbomachinery Society of Japan, Vol.17-No.4, pp.222-231, 1989 (in Japanese).

[16] S.Akishita, and K.Ohtsuta, "Broad band noise from an isolated two dimensional airfoil," 10th AIAA Aeroacoustics Conference, Seattle, WA, AIAA Paper. 86-1948, 1986.